Impact of land use change on the diurnal cycle climate of the Canadian Prairies

Alan K. Betts,[1] Raymond Desjardins,[2] Devon Worth,[2] and Darrel Cerkowniak[3]

Received 9 August 2013; revised 30 September 2013; accepted 11 October 2013; published 11 November 2013.

[1] This paper uses hourly observations from 1953 to 2011 of temperature, relative humidity, and opaque cloud cover from 14 climate stations across the Canadian Prairies to analyze the impact of agricultural land use change on the diurnal cycle climate, represented by the mean temperature and relative humidity and their diurnal ranges. We show the difference between the years 1953–1991 and 1992–2011. The land use changes have been largest in Saskatchewan where 15–20% of the land area has been converted in the past four decades from summer fallow (where the land was left bare for 1 year) to annual cropping. During the growing season from 20 May to 28 August, relative humidity has increased by about 7%. During the first 2 months, 20 May to 19 July, maximum temperatures and the diurnal range of temperature have fallen by 1.2°C and 0.6°C, respectively, cloud cover has increased by about 4%, reducing surface net radiation by 6 W m^{-2}, and precipitation has increased. We use the dry-downs after precipitation to separate the impact of cloud cover and show the coupling between evapotranspiration and relative humidity. We estimate, using reanalysis data from ERA-Interim, that increased transpiration from the larger area of cropland has reduced the surface Bowen ratio by 0.14–0.2. For the month on either side of the growing season, cloud cover has fallen slightly; maximum temperatures have increased, increasing the diurnal temperature range and the diurnal range of humidity.

Citation: Betts, A. K., R. Desjardins, D. Worth, and D. Cerkowniak (2013), Impact of land use change on the diurnal cycle climate of the Canadian Prairies, *J. Geophys. Res. Atmos.*, *118*, 11,996–12,011, doi:10.1002/2013JD020717.

1. Introduction

[2] In the past 30 years there has been a major change in land use over the Canadian Prairies, specifically the conversion of more than five million hectares of summer fallow (where the land was left bare for 1 year) to continuous annual cropping. The large increase in the area of cropland has increased summer transpiration. This has modified the warm-season climate over the Prairies, particularly in the period from 15 June to 15 July [*Gameda et al.*, 2007]. There has been a decrease in mean daily maximum temperature and the diurnal temperature range, a decrease in the incoming solar radiation, and an increase in precipitation, particularly during mid-July at the peak of the growing season. *Raddatz* [1998] suggested that increased evapotranspiration (ET) during the height of the growing season, which enhances the potential for moist deep convection, is likely to have resulted in more frequent and severe precipitation events.

[3] This paper explores these links between climate change, land use, and the summer diurnal cycle climate using hourly observations of temperature, relative humidity, and opaque cloud cover, and daily precipitation data since 1953 from 14 climate stations across the Canadian Prairies. Our objective is to understand the impact of land use change on the diurnal climate, represented by the mean temperature and relative humidity and their diurnal ranges. We will show how the seasonal cycle of the diurnal climate has changed with land use. We will compare the change in the seasonal cycle over the Prairies with the seasonal cycle over the boreal forest to the north, which has not changed.

[4] There is an extensive literature on the impact of ecosystem and crop phenology of the seasonal cycle, especially the spring transition when ET increases steeply with leaf emergence [*Schwartz and Karl*, 1990; *Schwartz*, 1994, 1996; *Schwartz et al.*, 2012; *Fitzjarrald et al.*, 2001; *Freedman et al.*, 2001].

[5] *Pielke* [2001] reviews the many links between surface moisture, land-surface heat fluxes, and cumulus convective rainfall. *Lyons et al.* [1996] discuss using satellite observations the change in the surface energy balance that has resulted from the replacement of native vegetation with annual winter crops in southwestern Australia. They found a marked reduction in the sensible heat flux to the atmosphere during winter and spring that may be related to the decrease in winter rainfall observed throughout the agricultural region. *Wang et al.* [2013] have simulated the annual cycle of ET for the entire Canadian landmass for the period 1979–2008 at $1 \times 1\,km^2$

[1]Atmospheric Research, Pittsford, Vermont, USA.
[2]Agriculture & Agri-Food Canada, Ottawa, Ontario, Canada.
[3]Agriculture & Agri-Food Canada, Saskatoon, Saskatchewan, Canada.

Corresponding author: A. K. Betts, Atmospheric Research, Pittsford, VT 05763, USA. (akbetts@aol.com)

2169-897X/13/10.1002/2013JD020717

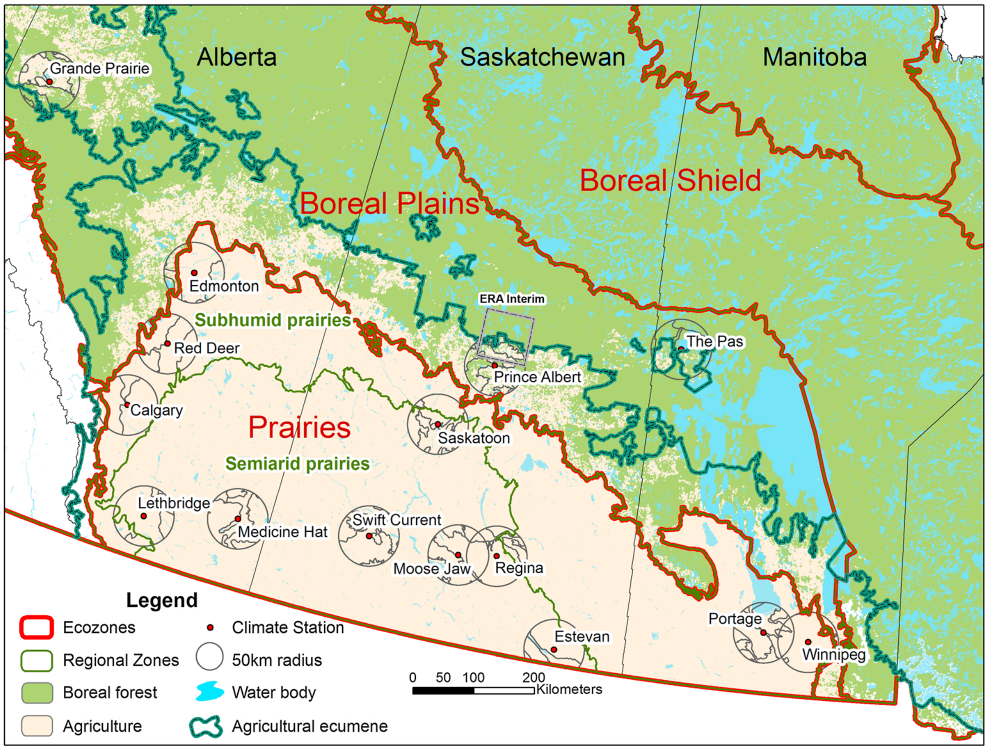

Figure 1. Climate station locations, Canadian Ecozones, regional zones, agricultural regions, and boreal forest.

spatial resolution using the Ecological Assimilation of Land and Climate Observations model driven by remote sensing land-surface data and gridded meteorological forcing products. Vegetation types and leaf area index are characterized using satellite data from the year 2000. *Betts et al.* [2007] contrasted the surface energy balance and cloud feedbacks between agricultural land and boreal forest in the transition zone between the Prairies and forest in Saskatchewan.

[6] There have been many modeling studies of the impact of land use change on the water and energy cycle, mostly dealing with the conversion of natural landscapes to cropland. *Bounoua et al*. [2002] used two 15 year climate simulations to show that in temperate latitudes, where human modification of the landscape has converted large areas of forest and grassland to cropland, conversion cools canopy temperatures up to 0.7°C in summer from the increased latent heat flux of crops during the growing season and up to 1.1°C in winter from increased albedo. *Diffenbaugh* [2009], using a high-resolution nested climate modeling system, showed statistically significant warm-season cooling, driven by changes in both surface moisture balance and surface albedo, in regions where crop/mixed farming has replaced short grass (in areas of the Great Plains) and interrupted forest (in areas of the Midwest and southern Texas) and with regions of irrigated crops (in the western United States). *Mishra et al.* [2010] used historic, present, and projected future land cover data and observed meteorological forcing data for 1983–2007 over Wisconsin (U.S.) to drive a variable infiltration capacity model. They found that a full forest-to-cropland conversion reduced annual average net radiation and sensible heat flux, partly due to the large impact of increased snow albedo in winter and spring. Forest-to-cropland conversion also reduced annual ET, although the latent heat flux increased in summer. *Lu and Kueppers* [2012] discuss the surface energy partitioning over four dominant vegetation types across the United States by comparing flux tower observations with a coupled regional climate model. A simulation of the hydroclimatic impacts of projected Brazilian sugarcane expansion by *Georgescu et al*. [2013] shows a cooling of order 1°C during the peak of the growing season from increased evapotranspiration and a warming of similar magnitude after harvest. *Christidis et al*. [2013] explore the role of land use change on daily temperatures and find that loss of trees and increase of grassland since preindustrial times has caused an overall cooling trend in both mean and warm extreme temperatures.

[7] The climate data we analyze here show that the coupled system response of the diurnal and seasonal climate to changes in agricultural land use are consistent with those seen in models, and they provide greater detail. On the other hand, we have no direct data on the surface Bowen ratio (BR) or ET. A preceding paper [*Betts et al*., 2013] used the first 40 years of these data to address the cloud radiative forcing of the diurnal cycle climate over the seasonal cycle. We will use their results to separate the impact of clouds on the surface energy budget from the changes in BR and relative humidity (RH), coming from increased annual cropping. One useful surrogate is the dry-down after rain events, which show the response of the local diurnal climate to falling ET. To estimate the coupling between RH and BR, we will use hourly model data with computed surface fluxes from the European Centre reanalysis known as ERA-Interim [*Dee et al*., 2011]. These were archived for a grid point, shown later in Figure 1, for the Boreal Ecosystem-Atmosphere Study (BOREAS) and the Boreal Ecosystem Research and Monitoring Sites (BERMS) in Saskatchewan.

[8] Our analysis shows that increased annual cropping has changed the seasonal diurnal climate of the Canadian

Table 1. Airport Climate Stations: Location and Elevation

Station Name	Station ID	Province	Latitude	Longitude	Elevation (m)
Red Deer[a]	3025480	Alberta	52.18	−113.62	905
Calgary[a]	3031093	Alberta	51.11	−114.02	1084
Lethbridge[b]	3033880	Alberta	49.63	−112.80	929
Medicine Hat	3034480	Alberta	50.02	−110.72	717
Grande Prairie[a]	3072920	Alberta	55.18	−118.89	669
Regina[a]	4016560	Saskatchewan	50.43	−104.67	578
Moose Jaw	4015320	Saskatchewan	50.33	−105.55	577
Estevan[a]	4012400	Saskatchewan	49.22	−102.97	581
Swift Current[b]	4028040	Saskatchewan	50.3	−107.68	817
Prince Albert[a]	4056240	Saskatchewan	53.22	−105.67	428
Saskatoon[a]	4057120	Saskatchewan	52.17	−106.72	504
Portage-Southport	5012320	Manitoba	49.9	−98.27	270
Winnipeg[a,b]	5023222	Manitoba	49.82	−97.23	239
The Pas[a,b]	5052880	Manitoba	53.97	−101.1	270

[a]Complete data sets.
[b]Stations with downward shortwave radiation.

Prairies, which furthers our understanding of the seasonal climate transitions [*Betts*, 2011a] at the beginning and end of the growing season. The local coupling between land surface, boundary layer, clouds, and phenology on seasonal timescales is coupled to changes in regional and global climate. Where possible, we will identify local coupled processes as a guide to understanding the changing climate of the Prairies and provide a benchmark for evaluating the realism of climate model simulations of the past 60 years.

[9] Section 2 reviews the climate station data and the changes in agricultural land use and summarizes the results of *Betts et al*. [2013] on the warm-season coupling between cloud cover and the diurnal climate. Section 3 shows the impact of the change in land use across the Prairies on the annual cycle of temperature, *T*, relative humidity, RH, and their diurnal ranges, along with opaque cloud cover. Section 4 analyzes the surface and cloud radiative forcing of the diurnal cycle climate and the dry-downs after rain events and shows comparisons with ERA-Interim grid point data. Section 5 uses the ERA-Interim data to estimate the land-surface coupling between BR and RH and shows the mean warm-season change in temperature, humidity, cloud, precipitation, and surface fluxes with land use change in the Saskatchewan Prairies. Section 6 presents our conclusions.

2. Data and Background

2.1. Climate Stations and Ecozones

[10] We used data from the 14 climate stations listed in Table 1. These have hourly data, starting in 1953 for all stations, except Regina and Moose Jaw which start in 1954. The stations are all at airports. The 11 southern stations from 49 to 52°N are in agricultural regions, and the 3 most northern stations (The Pas, Prince Albert, and Grand Prairie) are either in or close to the boreal forest. We generated a file of daily means for all variables (from the 24 hourly values) and extracted and appended to each daily record the corresponding hourly data at the times of maximum and minimum temperature ($T_{\max}$ and $T_{\min}$). We merged daily total precipitation and daily snow depth. This is our reduced diurnal cycle climate data set [*Betts et al*., 2013]. In the first 40–50 years there are very few missing hourly observations. Nine stations, marked correspondingly in Table 1, have maintained a complete hourly record to the present, while five have been reduced to daytime observations in recent years, which breaks the continuity and usefulness of their records because we can no longer calculate a true daily mean.

[11] Figure 1 shows the distribution of the climate stations across Ecozones in western Canada. Ecozones are the broadest group within the Canadian ecological stratification hierarchy. They are further subdivided into ecoregions and ecodistricts, each level providing increasing scale and distinction of biotic (e.g., soil and vegetation) and abiotic (e.g., climate and topography) features and information. A web visualization tool exists for these ecological subdivisions [*Ecodistrict*, 2013]. Using ecoregions, the prairie ecozone was subdivided into two regional zones, the semiarid prairies and subhumid prairies. These subdivisions represent differences in climate deemed sufficient to significantly affect the nature and management of agriculture. The 50 km radius circles around each station were used to generate local averages of the ecodistrict crop data (see next section). Land use averages were also generated within the agricultural ecumene for each provincial ecological zone (boreal plains ecozone and semiarid/subhumid prairie regional zones). Agriculture is only a small fraction of the agricultural ecumene within the much larger boreal plains ecozone (Figure 1).

2.2. Trends in Agricultural Land Use Around the Climate Stations

[12] The ecodistrict crop data [*AAFC*, 2011] were interpolated and averaged in the 50 km radius region centered on each climate station shown in Figure 1. The trends for cropland (red), pasture (green), and summer fallow (blue) around each climate station by province are shown in Figure 2.

[13] Since the 1970s there has been a general increase in cropland and a decrease in summer fallow. This transition has been largest in Saskatchewan, where in the 1960s and 1970s the summer fallow exceeded 30% of land area around Regina, Estevan, and Swift Current, but since 1991 this has fallen sharply to a current value around 5%. In Manitoba, the increase in cropland occurred before 1981 and percent of summer fallow was only around 10% in the 1960s.

[14] We chose to average land use over this 50 km radius because we are interested in the impact of land use change on the diurnal cycle in the growing season in the coupled system with a changing atmospheric boundary layer and cloud field. This is nonlocal response. The 100 km scale

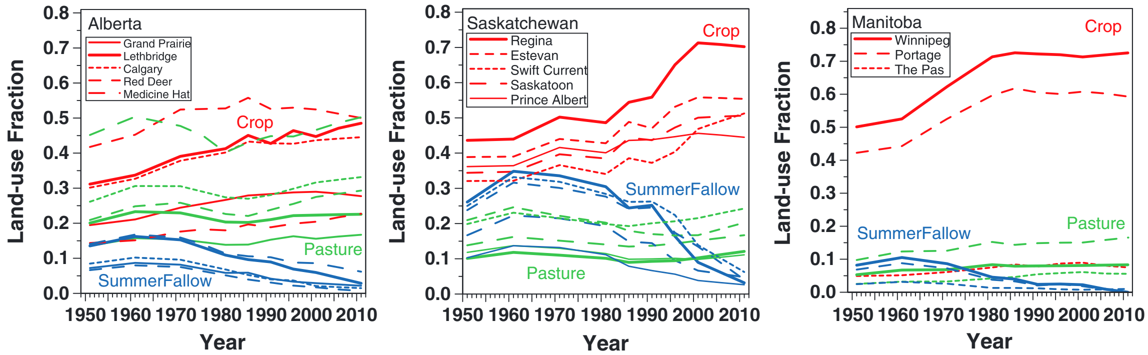

Figure 2. Trends in cropland, pasture, and summer fallow for 50 km radius region centered on each climate station.

corresponds to an advection time of order 7 h at a wind speed of 4 m s^{-1}. The next section averages up to the larger scales of the ecological zones for comparison.

2.3. Ecological Zone Changes in Summer Fallow and Cropland

[15] Figure 3 shows how the percent of the land area in annual and perennial crops, total cropland, pasture, and summer fallow within the agricultural ecumene has changed over the 60 years. Note that cropland is not exactly the sum of annual and perennial crops, because they are aggregated based on crop-specific variables in the census; reporting is farm-specific, and some information is suppressed at the lower levels to maintain confidentiality. Summer fallow is further subdivided into averages over the ecological zones for each province shown in Figure 1. We see that the drop in summer fallow, shown in Figure 2 for the 50 km circle regions around the climate stations, is broadly representative of the provincial ecological zones. Saskatchewan has shown the steepest drop from peaks around 25% in the semiarid and subhumid prairies in the 1960s, while in Alberta and Manitoba, the peak in summer fallow was much smaller. These decreases in summer fallow have been matched largely by a corresponding increase in cropland, both annual crops and perennial crops that are cropped annually.

2.4. Coupling Between the Diurnal Cycle, Clouds, and Precipitation in the Warm Season

[16] The Canadian hourly climate data from the early 1950s to the present are very useful because they contain hourly observations of opaque cloud cover in tenths. These cloud data show the land-surface-cloud coupling over both the diurnal and seasonal cycles [*Betts et al.*, 2013]. These opaque cloud data are of such good quality that we were able to calibrate them against multiyear longwave and shortwave radiation data (see section 4 later).

[17] Our analysis framework is based on the concept of the land-surface diurnal cycle climate, introduced by *Betts and Ball* [1995, 1998] for a grassland study and used by *Betts et al.* [2001] for a boreal forest study and by *Betts* [2004] to discuss hydrometeorology in global models. For individual days, the diurnal cycle is a combination of local processes and synoptic scale advection. However, if sufficient data are composited, the climate structure representative of the local energy balance emerges from the synoptic variability. This is especially true in summer, when the solar forcing is large.

[18] We characterize the diurnal cycle by the diurnal temperature range between maximum and minimum temperatures ($T_{\max}$, $T_{\min}$)

$$\mathrm{DTR} = T_{\max} - T_{\min} \tag{1}$$

and the diurnal range of RH which can be approximated in the warm season as

$$\Delta\mathrm{RH} = \mathrm{RH} : T_{\min} - \mathrm{RH}{:}T_{\max} \tag{2}$$

[19] This is because in the typical diurnal cycle, maximum RH is generally at $T_{\min}$ at sunrise and the minimum RH is at $T_{\max}$ in the afternoon [see *Betts et al.*, 2013].

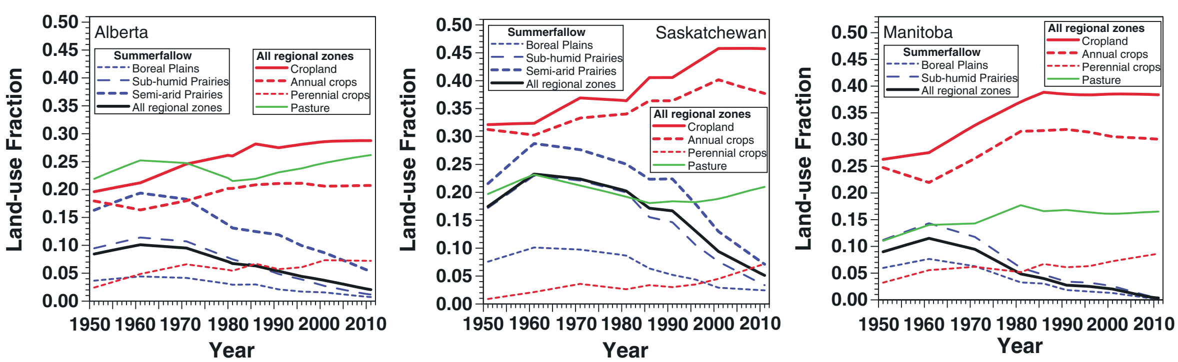

Figure 3. Trends in annual and perennial crops, total cropland, pasture, and summer fallow subdivided by provincial regional ecological zones.

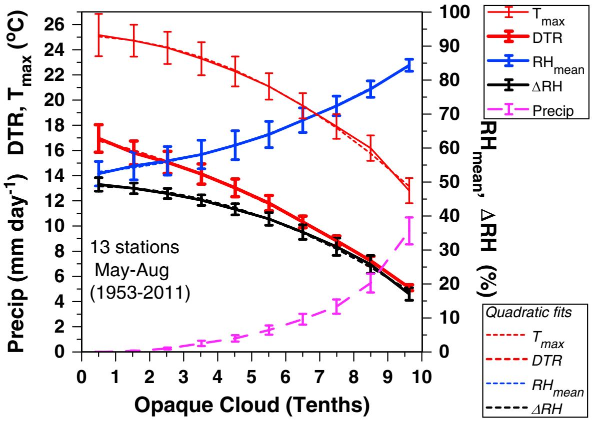

Figure 4. Climatological dependence of T_{max}, DTR, RH_{mean}, ΔRH, and precipitation on opaque cloud for May to August, with quadratic fits.

[20] Figure 4 shows that T_{max}, diurnal temperature range (DTR), and ΔRH fall, and daily mean RH (RH_{mean}) and daily precipitation increase with increasing opaque cloud cover. Of the 14 stations in Table 1, we have omitted Portage-Southport where the precipitation data is incomplete. The relatively small standard deviations across the means for the 13 Prairie stations show that this diurnal climate structure is representative of the Prairies. Note that standard deviations of DTR ($\leq\pm1$°C) and ΔRH ($\approx\pm2$%) are both smaller than for T_{max} and RH_{mean}.

[21] The barely visible dotted lines, which we will use to represent the climatology of this warm-season coupling to cloud cover, are these quadratic fits.

$$T_{max}:\ \text{fit} = 25.10 - 0.043\ \text{Opaque Cloud} - 0.1243\ \text{Opaque Cloud}^2 \tag{3a}$$

$$\text{DTR}:\ \text{fit} = 17.11 - 0.624\ \text{Opaque Cloud} - 0.0641\ \text{Opaque Cloud}^2 \tag{3b}$$

$$\text{RH}:\ \text{fit} = 52.71 + 0.544\ \text{Opaque Cloud} + 0.2813\ \text{Opaque Cloud}^2 \tag{3c}$$

$$\Delta\text{RH}:\ \text{fit} = 48.82 + 0.148\ \text{Opaque Cloud} - 0.3481\ \text{Opaque Cloud}^2 \tag{3d}$$

[22] We shall take these averages for the period May–August as representative of the growing season climatology. In section 4, we will use them as a reference when we separate the impacts of cloud and land-surface processes on the diurnal cycle.

[23] In fact, *Betts et al.* [2013] showed that the coupling between diurnal climate and cloud cover has very distinct warm and cold season states. The diurnal ranges of temperature and ΔRH in Figure 4 are representative of the months from April to October. There are rapid transitions to a winter state that occur typically in November and March, when temperature falls below freezing and the ground becomes snow covered. In the annual cycle of the diurnal climate shown in section 3, these winter transitions are sharply delineated by a large drop/rise in ΔRH.

[24] For nine stations our 24 h meteorological data extend until early July 2011. We exclude days when nighttime data are missing. This affects five stations: Swift Current for 1980–1986, Portage-Southport after 1991, Moose Jaw after 1998, and Lethbridge and Medicine Hat after 2005. Our daily precipitation record ends in 1994 for Swift Current, in 2008 for Regina and Winnipeg, and in 2009 for Saskatoon. Precipitation is missing at Portage-Southport before 1996.

3. Change of Annual Cycle of *T*, DTR, RH, ΔRH, and Opaque Cloud With Land Use

[25] We will first focus on the prairie region of Saskatchewan, where the land use change from summer fallow to annual cropping has been the largest (Figures 2 and 3). The annual cycle will be shown using 10 day means of the daily data, and the long time series will be partitioned into two segments, 1953–1991 and 1992–2011, to capture the sharp reduction in summer fallow in the past two decades. The plots are based on day of year (DOY). Where we give corresponding dates, they are for DOY in nonleap years. We use the framework, discussed in section 2.4, for characterizing the diurnal cycle in terms of *T* and RH. Later, we will discuss the impact on mixing ratio and convective instability (section 3.2) and the links between changes in RH and changes in ET (section 4.3).

3.1. Change in the Annual Cycle at Saskatoon, Regina, and Estevan

[26] Figure 5 shows three stations, Saskatoon, Regina, and Estevan, which have 24 h data through the whole period. For each station the left plot shows temperature and DTR, and the right plot RH_{mean}, ΔRH, and opaque cloud (in tenths). Although the changes over the annual cycle are complex, there are similarities across the three stations. The winter warming is visible between the two time periods, but otherwise DTR, RH_{mean}, and ΔRH show no systematic differences in the cold season. Agricultural land use has less impact when snow covers the ground.

[27] There are two spring transitions [*Betts*, 2011a]. The first is the sharp transition after DOY = 85 (26 March), which is the average date of snowmelt [*Betts et al.*, 2013], when there is a sharp rise of DTR and ΔRH and a fall of RH_{mean}. The diurnal cycle of temperature and RH change from a cold-season to a warm-season state [*Betts et al.*, 2013]. The soil then dries, and with the solar zenith angle decreasing rapidly, temperature rises and humidity falls to a minimum. Figure 4 shows that RH_{mean} reaches a climatic minimum about 5–6 weeks after snowmelt.

[28] The peak in DTR and minimum in RH_{mean} around DOY = 135 (15 May) mark the beginning of the second spring transition that occurs with the green-up of the landscape and the spring growth of annual crops [*Schwartz and Karl*, 1990; *Schwartz*, 1994, 1996; *Fitzjarrald et al.*, 2001; *Freedman et al.*, 2001]. In the recent period the peaks in DTR and trough in RH_{mean} are earlier by 10–20 days. This is consistent with the earlier start to the growing season by several days per decade [*Qian et al.*, 2009, 2012].

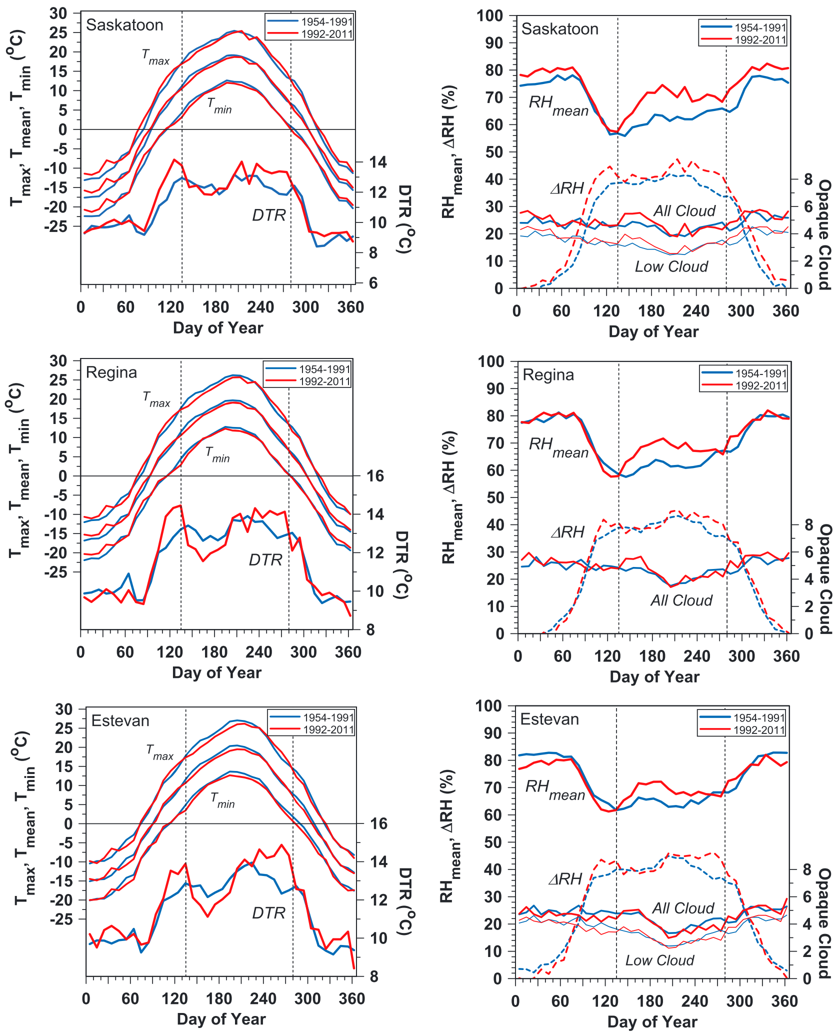

Figure 5. Change in annual cycle of (left) T_{max}, T_{mean}, T_{min}, and DTR and (right) RH_{mean}, ΔRH and opaque cloud for Saskatoon, Regina, and Estevan.

However, this transition depends on the planting dates of annual crops, as well as the impact of a warming winter climate on the spring regrowth of perennial crops and the natural ecosystem [*Betts*, 2011b]. The average seeding date for spring wheat in Saskatchewan for the period 1952–1984 was 11 May, with a range of several weeks depending on soil and climate conditions in spring [*Bootsma and De Jong*, 1988].

[29] For the period from 20 May to 27 August ($140 \leq \text{DOY} < 240$), which we will consider to be the growing season, the seasonal cycle shows a distinct increase in RH_{mean} between the two periods that is consistent with increased transpiration from the conversion of summer fallow to cropland. Opaque cloud falls from DOY = 150, when the peak is noticeably higher in the recent period, to a minimum around

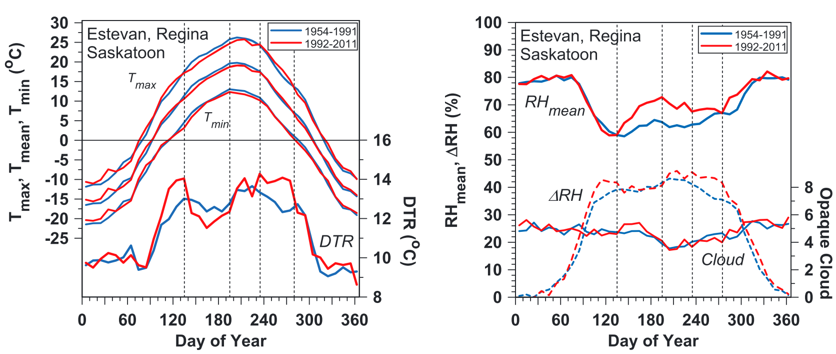

Figure 6. As in Figure 5 for mean of three stations in Saskatchewan.

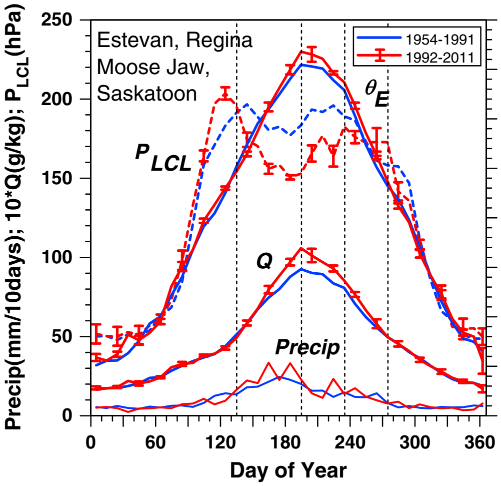

Figure 7. Mean seasonal change with land use in θ_E, P_{LCL}, and Q, at the time of T_{max}, and daily precipitation.

DOY = 210 (29 July). We will discuss these summer differences in more detail below with Figure 6 and in section 5.

[30] Note that in the recent period after 1991, T_{max}, DTR, and ΔRH are higher, both before the growing season (10 April to 19 May, $110 \leq \text{DOY} < 139$) and after the end of the growing season, 28 August to 6 October ($240 \leq \text{DOY} < 279$). A fall transition follows as DTR and ΔRH decrease from 7 October to 16 November (DOY = 320), the mean date of the first lasting snow cover in Regina [*Betts et al.*, 2013].

[31] Figure 6 shows the mean for these three stations: Saskatoon, Regina, and Estevan. We show four dotted lines to visually link the changes in different variables at DOY = 135, 195, 235, and 280, corresponding to 15 May, 14 July, 23 August, and 7 October. This change in the seasonal cycle from the early (mean of 1972) to later period (mean of 2001) has these characteristics:

[32] 1. For $140 \leq \text{DOY} < 200$ (20 May to 18 July), the recent period has a DTR that is lower by −0.6°C, with T_{max} lower by −1.2°C and T_{min} lower by −0.6°C.

[33] 2. For $140 \leq \text{DOY} < 240$ (20 May to 27 August), RH_{mean} averages 7% higher in the recent period and reaches a peak at DOY = 195 (14 July).

[34] 3. For $140 \leq \text{DOY} < 200$ (20 May to 18 July), mean opaque cloud is higher by 4% on average in the recent period.

[35] There are two other stations in Saskatchewan which lack nighttime observations in recent years: Moose Jaw after 1997, and Swift Current from 1980 to 1986 and on some days in later years. We have computed bias corrections for the missing nighttime data by subsampling the first four decades of complete record. With these corrections, Moose Jaw and Swift Current then show similar changes to those seen in Figure 5, but we do not include them in the Figure 6 mean because of the added uncertainty of these bias corrections.

3.2. Afternoon Change in Midsummer θ_E, P_{LCL}, and Q at the Time of T_{max}

[36] Figure 7 shows the mean change of four Saskatchewan stations between the two periods in equivalent potential temperature, θ_E and P_{LCL}, the pressure height to the lifting condensation level (LCL), mixing ratio, Q, all at the time of T_{max}, together with daily precipitation. We have added Moose Jaw because it has precipitation data (1954–2011) and daytime data at the time of T_{max}. The standard deviations shown on the 1992–2011 mean curve are for the differences across the four stations between the two time periods. The impact of the change in land use is visible during the growing season. In the recent period from 1992 to 2011, the higher RH:T_{max} over the Prairies from increased evapotranspiration

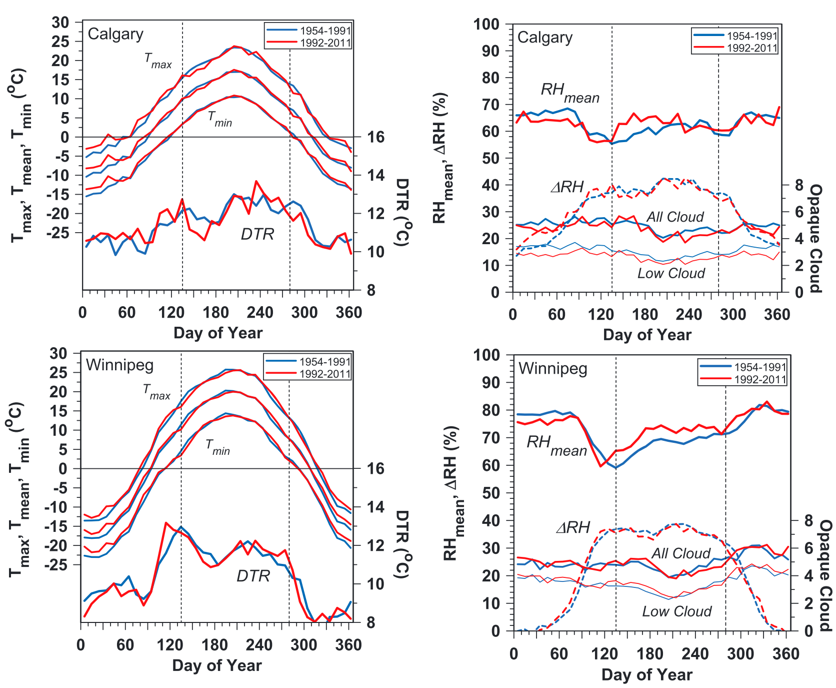

Figure 8. As in Figure 5 for Calgary and Winnipeg.

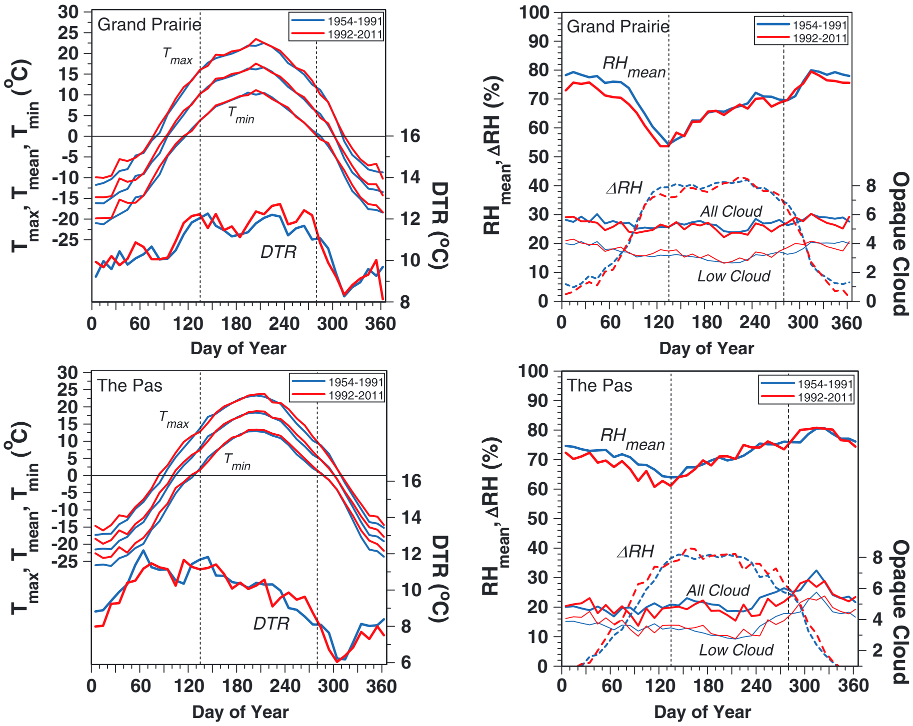

Figure 9. As in Figure 5 for Grand Prairie and The Pas.

gives P_{LCL} that is lower by 24 hPa for $140 \leq DOY < 240$, and for $160 \leq DOY < 260$ a θ_E that is higher by 1.8 K and a Q that is higher by 9.4%.

[37] Precipitation over the Prairies in recent decades has increased, especially from 15 June to 15 July ($166 \leq DOY < 196$) during the period of peak crop transpiration [*Gameda et al.*, 2007]. Precipitation is a noisy variable, but Figure 7 shows a mean precipitation increase of 24% in the early growing season ($140 \leq DOY < 200$), coincident with the fall of P_{LCL}. This suggests that local evaporation-precipitation feedback may be increasing precipitation. Almost all summer days have low-level boundary layer cloud, so P_{LCL} generally corresponds to the pressure height of cloud base. A lower cloud base and higher θ_E favors deep convection, and an increase of Q for air lifted to cloud base is consistent with an increase in precipitation. *De Ridder* [1997] showed that θ_E generally increases with increasing evaporative fraction, which increases the potential for precipitating convection. *Raddatz* [1998] also suggested that increased ET during the height of the growing season, which enhances the potential for moist deep convection, is likely to have resulted in more frequent and severe precipitation events. *Raddatz and Cummine* [2003] have suggested there is a link between increased ET from the agro-ecosystem, increased boundary layer moisture, and the number of tornado days over the Prairies.

[38] One historic reason for summer fallow was to reduce ET and conserve soil water in a dry climate. However, the increase of ET from the conversion to cropland may have increased precipitation. This near balance in summer between ET and precipitation over northern continental regions, including Canada, has been seen in global model simulations over a wide range of initial soil moisture conditions [*Betts*, 2004]. For the Prairies, *Wang et al.* [2013] show that there is a close balance between precipitation and ET over the annual cycle.

3.3. Seasonal Cycle Changes for Calgary and Winnipeg

[39] Figure 8 shows the corresponding changes for two other Prairie climate stations, Calgary and Winnipeg. The spring peak in DTR and minimum in RH_{mean} are again earlier in recent decades. The growing season changes are similar to those in the province of Saskatchewan but smaller. For $140 \leq DOY < 200$ (20 May to 18 July) T_{max} falls -0.8°C at Calgary and -0.6°C at Winnipeg. For $140 \leq DOY < 230$ (20 May to 18 August), RH_{mean} averages 4.5% higher in the recent period. For $140 \leq DOY < 200$ (20 May to 19 July), mean opaque cloud is higher by 0.2 tenths on average in the recent period for Winnipeg. At Calgary the changes in cloud are small, and the low cloud observations are systematically lower after the mid-1970s.

3.4. Northern Boreal Forest Stations

[40] Figure 9 shows the corresponding changes for two northern climate stations. At Grand Prairie, there has been a small shift from summer fallow to annual cropping (Figure 2), but the agricultural region is small (Figure 1) and embedded in the boreal forest. The Pas is primarily boreal forest, and the agricultural land use is small and has changed little.

[41] The periods before and after 1991 show little difference in growing season RH_{mean}, T_{max}, or T_{min}. The monotonic rise of RH_{mean} from a spring minimum, when transpiration is low until the soil warms, to a fall maximum is characteristic of the boreal forest [*Betts et al.*, 2001] and quite distinct from the growing season peak with annual crops seen in Figure 6. There is some indication of an earlier minimum in RH, which would be consistent with earlier spring melt in a warming climate.

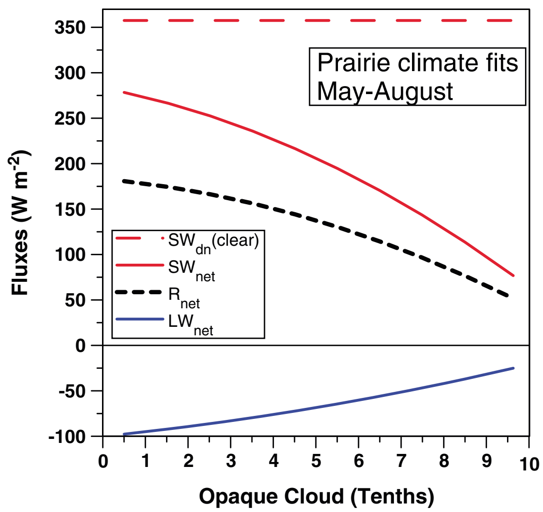

Figure 10. Dependence of radiative fluxes on opaque cloud cover using (7) to (11).

3.5. Summary of the Annual Cycle Changes

[42] Figures 5, 6, 8, and 9 show warming in winter (December to March). For the nine stations with complete data records, T_{mean} increases by 1.09 ± 0.57°C between the periods before and after 1991, reflecting the warming of the Canadian winter climate. In the early part of the growing season from $140 \leq \mathrm{DOY} < 200$ (20 May to 18 July), the Prairie stations show a cooling, moistening signal in the recent period. This is largest in Saskatchewan, a drop in T_{max} of -1.2°C and in T_{min} of -0.6°C and a rise of mean RH_{mean} of 7%. The conversion of summer fallow to cropland on nearly 20% of the agricultural land has been largest there. The shift to a cooler, moister early growing season has been smaller at Calgary and Winnipeg, where the reduction in summer fallow has been smaller. The climate stations in the boreal forest show no change in the growing season in T_{max}, T_{min}, or RH_{mean}. We will now show evidence that the changes in the growing season climate are consistent with increases in ET associated with a larger coverage of cropland.

4. Surface and Cloud Forcing of the Diurnal Cycle Climate

[43] The surface energy balance between surface shortwave, longwave, and net radiation fluxes (SW_{net}, LW_{net}, and R_{net}) and the sensible, latent and ground heat fluxes (H, λE, and G) can be written

$$SW_{net} + LW_{net} = R_{net} = H + \lambda E + G \tag{4}$$

[44] Changes in land use, as well as soil moisture, directly change the surface partition of the net radiation, represented by the Bowen Ratio (BR) or the evaporative fraction (EF) defined as

$$\mathrm{BR} = H/\lambda E \tag{5}$$

$$\mathrm{EF} = \lambda E/(H + \lambda E) \tag{6}$$

[45] The shift from summer fallow to annual cropping will increase transpiration and EF (and decrease BR) during the growing season [*Gameda et al.*, 2007]. We have no direct measures of the surface energy partition, represented by 5 or 6; although Figures 5, 6, and 7 show that land use change has altered the seasonal diurnal cycle and increased RH_{mean}.

[46] However, the important role of clouds on the net radiative forcing in (4) can be quantified. Four climate stations have measurements of incoming SW (SW_{dn}): Swift Current (1970–1994), The Pas (1972–1998), Winnipeg (1970–2000) and Lethbridge (1990–1998). Using these data and SW and LW data from the BOREAS/BERMS studies, *Betts et al.* [2013] calculated May–August fits for LW_{net} and effective cloud albedo (ECA) in terms of observed opaque cloud cover.

$$LW_{net} = -100.1 + 4.73\ \text{Opaque Cloud} + 0.317\ \text{Opaque Cloud}^2 \tag{7}$$

$$\mathrm{ECA} = 0.0681 + 0.0293\ \text{Opaque Cloud} + 0.00428\ \text{Opaque Cloud}^2 \tag{8}$$

where ECA is defined as the normalized reduction of the clear sky flux by clouds [*Betts and Viterbo*, 2005; *Betts*, 2009]

$$\mathrm{ECA} = (SW_{dn}(\mathrm{clear}) - SW_{dn})/SW_{dn}(\mathrm{clear}) \tag{9}$$

[47] Then

$$SW_{net} = (1 - \alpha_s)(1 - \mathrm{ECA})\ SW_{dn}(\mathrm{clear}) \tag{10}$$

[48] For the summer surface albedo, α_s, we will use a nominal 0.15 for the Prairies. For SW_{dn}(clear), we used the fit

$$SW_{dn}(\mathrm{clear}) = 68 + 321 \times (\cos(\pi(\mathrm{DOY} - 170))/365)^2 \tag{11}$$

[49] The relationships for SW_{net}, LW_{net}, and R_{net} derived from (7) through (11) are quadratic in opaque cloud cover, but quasi-linear in ECA [*Betts*, 2007; *Betts et al.*, 2013].

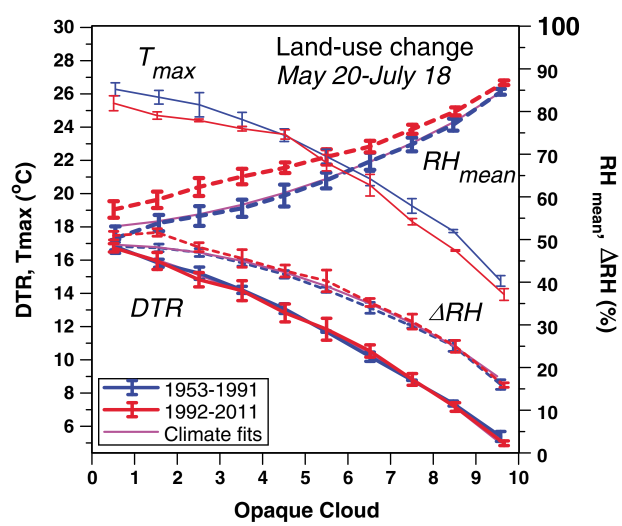

Figure 11. Dependence of T_{max}, DTR, RH_{mean} and ΔRH on opaque cloud cover showing impact of land use change during early growing season.

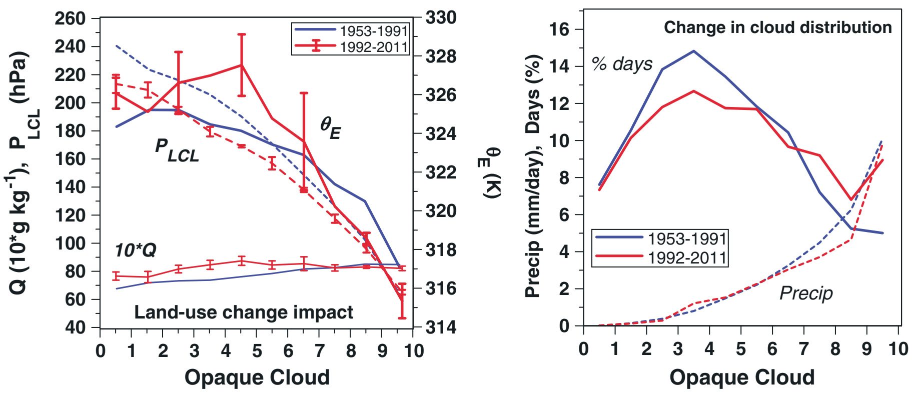

Figure 12. Impact of land use change of afternoon θ_E, P_{LCL}, and Q at time of (left) T_{max} and (right) daily cloud and precipitation distribution.

[50] Figure 10 shows the May–August mean fluxes as a function of opaque cloud cover for the Prairies using (7) to (11). The fact that climatologically the radiative drivers of the diurnal cycle depend just on cloud cover is of fundamental importance. It means that the stratification of the data by cloud can be used to separate the radiative forcing of the land-surface from the surface energy partition, represented by the BR, which depends on soil moisture and land use [*Betts*, 2007].

[51] Section 4.1 will separate the cloud coupling from the land use change in the diurnal cycle for the early growing season. Section 4.2 will use model data from ERA-Interim at a grid point in Saskatchewan to show how changes in the diurnal cycle are coupled to changes in the surface energy partition, as well as the dependence of SW_{net}, LW_{net}, and R_{net} on ECA. Section 4.3 will compare the diurnal cycle recovery as ET decreases in dry-downs after precipitation between the climate station data and the ERA-Interim data.

4.1. Change in Diurnal Cycle With Cloud and Land Use

[52] Figure 11 stratifies by opaque cloud cover the change in the diurnal cycle with land use using the daily data for the early growing season from $140 \leq DOY < 200$ (20 May to 18 July). It is a mean and standard deviation of the three Saskatchewan climate stations: Estevan, Regina, and Saskatoon (Figure 5). In the recent period T_{max} is cooler by about -0.7°C, RH_{mean} is moister by about +5%, while DTR and ΔRH are almost unchanged. This means the decrease of DTR seen in Figure 6 for the same time period is coupled to the increase of cloud cover. This cooler and moister surface state for the same cloud cover, and therefore the same R_{net}, is consistent with increased ET from the greater coverage of annual crops in the recent period. The May–August long-term climate fits for DTR, ΔRH, and RH_{mean} from (3) are barely visible as they are close to the curves for the 1953–1991 mean.

[53] Figure 12 (left) shows the early growing season impact of the land use change on θ_E, P_{LCL}, and Q at the time of afternoon T_{max}, and (Figure 12, right) the change in the daily cloud distribution and precipitation. The standard deviations shown on the 1992–2011 mean curve are for the differences between the two time periods. Cloud base, corresponding to P_{LCL}, is systematically lower in the recent period. Mixing ratio Q increases below 7/10 cloud and decreases above 7/10. Equivalent potential temperature, θ_E, a combination of Q and T_{max} (which Figure 11 shows is cooler since 1991), increases for opaque cloud cover between 2/10 and 7/10 and decreases for cloud > 7/10.

[54] Figure 12 (right) shows that in the recent period, the cloud distribution peak at 3.5 tenths is lower: there are fewer days with cloud fraction <7/10 and more days with > 7/10 cloud. This gives the increase in mean cloud cover seen in Figure 5 for $140 \leq DOY < 200$. The small changes in daily mean precipitation as a function of cloud, more for daily cloud cover <6/10 and less for cloud cover >6/10, are generally consistent with the sign of the change in afternoon θ_E. However, it is the shift in the cloud distribution to the right that gives the increase in precipitation seen in Figure 7.

4.2. Coupling Between ECA, Surface Fluxes, and Diurnal Cycle in Reanalysis

[55] Figure 13 shows the May-June-July-August (MJJA) coupling (Figure 13, top left) between ECA and the sensible and latent heat fluxes, H and λE, using data from ERA-Interim for the grid box north of Prince Albert, shown in Figure 1, and (Figure 13, top right) DTR, RH_{mean}, ΔRH, daily precipitation, and daily mean evaporation in millimeters. As cloud and precipitation increase, H falls steeply from 64 to -10 W m^{-2}, and the corresponding BR falls from 0.8 to -0.2. However, λE falls only from 82 to 46 W m^{-2} with increasing cloud, as increased ET with wet soils and wet vegetation partly compensate for the decreasing R_{net} (Figure 13, bottom left). Similar behavior was seen in surface flux observations for the BERMS Old Aspen, Old Black Spruce, and Old Jack Pine sites in Saskatchewan in *Betts et al.* [2006], who compared these data with a similar grid box from an earlier reanalysis known as ERA40. With increasing cloud and precipitation, DTR and ΔRH fall and RH_{mean} increases (Figure 13, top right). Evaporation is greater than precipitation for ECA <0.3. The quadratic fit to RH_{mean} shown will be used later in Figure 15.

[56] The corresponding changes with observed cloud and precipitation are shown (bottom right) for a four-station mean data set (Lethbridge 1990–1998, Swift Current 1970–1994, The Pas 1972–1998, and Winnipeg 1970–2000), where ECA was calculated from SW_{dn} measurements using 9 and 11. The standard deviations are across the four-station mean profiles. The observations show a quasi-linear dependence of DTR, RH_{mean}, and ΔRH on ECA, as noted in *Betts et al.* [2013]. We see that the coupling between ECA and diurnal cycle are broadly similar in observations and reanalysis,

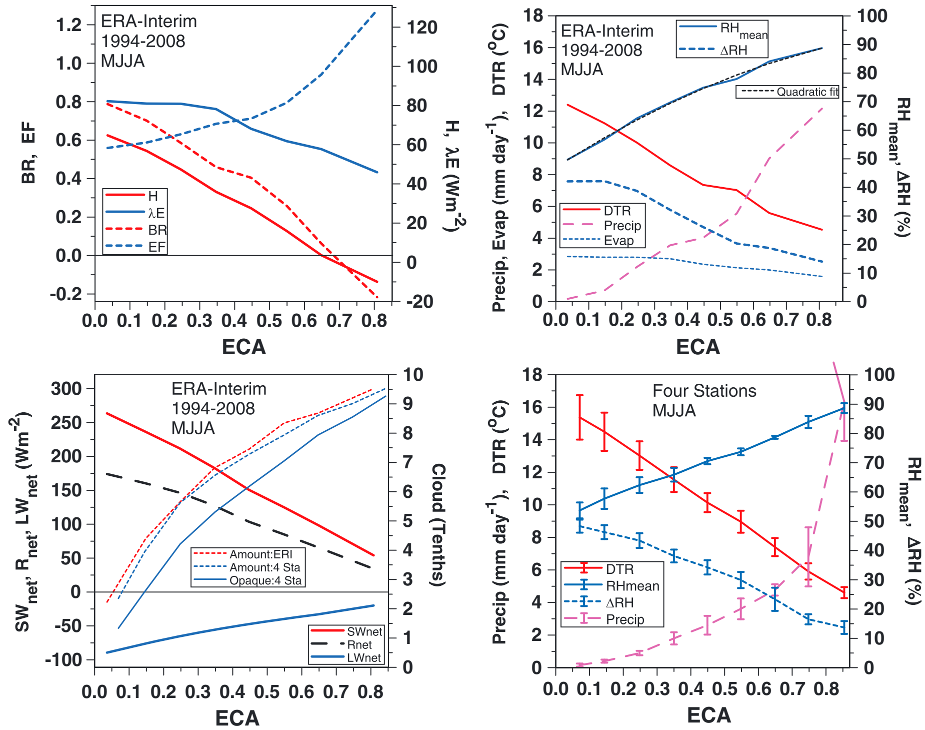

Figure 13. Dependence on ECA of (top left) H, λE, BR, and EF in reanalysis, (top right) DTR, RH_{mean}, ΔRH, daily precipitation, and daily mean evaporation in reanalysis, (bottom right) DTR, RH_{mean}, ΔRH, and daily precipitation for four-station mean, and (bottom left) SW_{net}, LW_{net}, R_{net}, and total cloud cover for reanalysis and total cloud cover and opaque cloud for four-station mean.

although there are differences in precipitation and the diurnal range at low cloud cover is smaller in the reanalysis. The reanalysis is a grid-box spatial mean on the edge of the boreal forest (Figure 1) for 1994–2008. The composite of the station observations covers the range of dates listed above (with 5 times as many days in total as ERA-Interim), but only one station, The Pas, is in the boreal forest.

[57] The radiative fluxes in the reanalysis (Figure 13, bottom left) show nearly linear changes with ECA [*Betts*, 2007]. We also show the increase of opaque cloud in the observations, which was the central focus of *Betts et al*. [2013], where its tight relationship to ECA was used to derive (8). The nonlinear increases in total cloud amount for reanalysis and observations are very similar.

[58] We conclude that although there are differences between data and the reanalysis (Figure 13, right column) in these composite climatologies, it is reasonable to infer that the decrease of BR coming from the steep fall of H with increasing ECA, decreasing R_{net}, and increasing precipitation is qualitatively representative of the Prairie data. *Betts et al.* [2006] noted similar surface flux dependence on ECA in comparisons between reanalysis and BERMS data for the boreal forest.

4.3. Dry-Down After Precipitation

[59] We examined the change in surface climate during the dry-down on days following precipitation. For the 13 Prairie stations with precipitation records, there are roughly 8600 precipitation events with more than 4 mm of rain during May–August 1953–2011. As noted in section 2.4, we lack precipitation data for the last few years for some stations.

[60] Figure 14 (left) shows a composite sequence for the 5 days following precipitation events. By definition it rains on day 0, and the mean precipitation is 12 mm. We terminate and restart the dry-down sequence if there is another rain event >4 mm within 5 days, so in the following 5 days the mean precipitation is very small, less than 0.5 mm day^{-1}. We see a rise of T_{max}, T_{mean}, and DTR and a fall of RH_{mean} and opaque cloud cover, while T_{min} falls for 2 days before recovering. Cold air advection behind frontal systems may contribute to this fall of T_{min}. Some variables, DTR, ΔRH, and cloud cover, adjust rapidly in the first 2 days after rain, while T_{max} and RH_{mean} have a slower recovery lasting out to 5 days.

[61] There are sufficient data to stratify the 5 day dry-downs by opaque cloud cover. Figure 14 (right) shows the distribution of T_{max}, DTR, ΔRH, and RH_{mean} as a function of cloud cover for the dry-down sequence. This separates the diurnal cycle dependence on changing cloud cover from the land-surface dependence that results from the fall of soil moisture during this composite dry-down. The precipitation curve is the mean of days 1–5, distributed by cloud cover. The heavy curves are the fits (3) representing the May–August climate mean from Figure 4.

[62] The light magenta curves are T_{max}, DTR, and RH_{mean} for the rain day, labeled 0. On day = 0 the DTR profile is near the climatological mean, but the T_{max} profile is warmer and the RH_{mean} profile is moister. The initial fall from day 0 to day 1 is large for T_{max} and DTR but very small for RH_{mean}. For DTR we see an increase at low cloud cover of about 1°C from days 1 to 2 and a rapid return of DTR, so that the days 3–5 mean is close to the season mean distribution. For ΔRH the differences from the season mean are tiny.

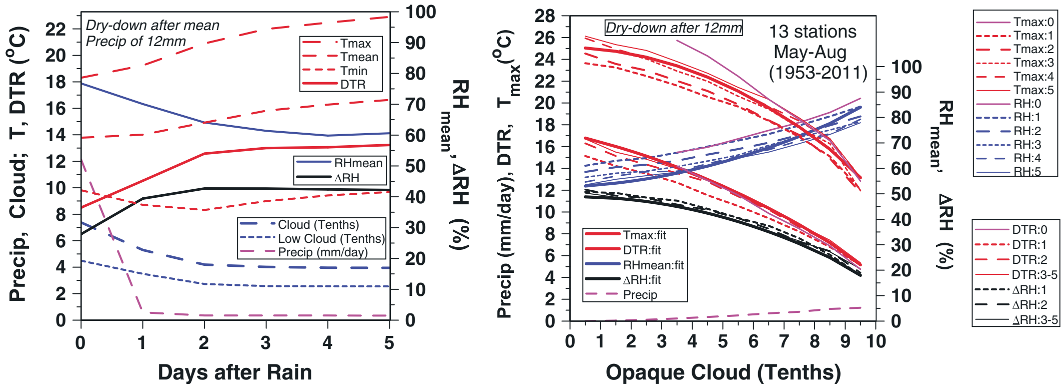

Figure 14. Dry-down after rain events: (left) change in temperature, DTR, RH_{mean}, ΔRH, cloud, and precipitation and (right) sequential day recovery toward climatology of the coupling of T_{max}, RH_{mean}, DTR, and ΔRH with cloud.

[63] For T_{max} and RH_{mean} we show the progression of the full 6 day sequence. T_{max} recovers over several days until by day 5 it is a little warmer than the climatology. RH falls by about 3% from days 1 to 2, decreasing to 2% for days 2 to 3, then 1% per day, until by day 5, the profile is close to the May–August climatology for cloud cover <7/10. At high cloud cover, the RH curves beyond day 1 fall below the climatology, but this is consistent with the fact that at 9/10 cloud, the climatology has a precipitation $\approx 9\,\mathrm{mm\,day^{-1}}$, whereas in our dry-down sequence, even with 9/10 cloud, precipitation is only $1.2\,\mathrm{mm\,day^{-1}}$.

[64] Now contrast these observations with the mean dry-down in ERA-Interim (ERI), where we have only 380 rain events in the 15 year period during May–August. Figure 15 (left) is very similar to Figure 14 (left). We see a rise of T_{max}, T_{mean}, and DTR and a fall of RH_{mean} and opaque cloud cover, while T_{min} falls for 2 days before recovering. Figure 15 (right) shows the change in the surface fluxes, R_{net}, H, and λE and RH_{mean} over the dry-down, binned by ECA. Because we have much less data, we have averaged the days 2–5, and we do not have the distribution over the full range of ECA. We show the May–August climatology of the coupling between ECA and RH_{mean} from Figure 13 (dashed line). In ERA-Interim, RH_{mean} on the rain days is much higher than the climatology and there is a large fall of RH_{mean} to the first day after rain, unlike the observations in Figure 14 (right). One possible explanation is that the model fast evaporation processes during rain, for example off wet canopies, are too rapid. There is a corresponding large fall in λE and rise of H in this first day after rain. In the model, RH_{mean} and λE fall further from day 1 to the day 2–5 mean, while H does not change.

[65] R_{net} (heavy black line) is a monotonic, almost linear function of ECA [*Betts*, 2007; *Betts et al*., 2013], which does not change over the dry-down sequence. So the changes in λE and H largely compensate. The rise in the ground flux as air temperatures warm partly compensates the drop in λE in the energy budget (not shown).

[66] It is reasonable to assume that ET falls as soil moisture falls in this dry-down sequence. Assuming surface stomatal conductance falls as soil moisture falls, the drop in RH across leaves and the wet surface will increase and near-surface RH will fall. We see this response of RH to soil water in equilibrium models where a vegetation model is coupled to a model for the cloudy boundary layer [e.g., *Betts et al*., 2004; *Betts and Chiu*, 2010] and in fully coupled forecast models [*Betts*, 2004; *Betts and Viterbo*, 2005]. We suggest that changes in RH_{mean} are a sensitive indicator of changes in surface stomatal conductance and hence ET. The drop of RH_{mean} at constant cloud cover in Figure 14 (right) is an indicator of falling ET, and conversely the increase in growing season RH_{mean} in Figures 5, 6, and 7 is an indicator of the increase of ET with the conversion of summer fallow to cropland.

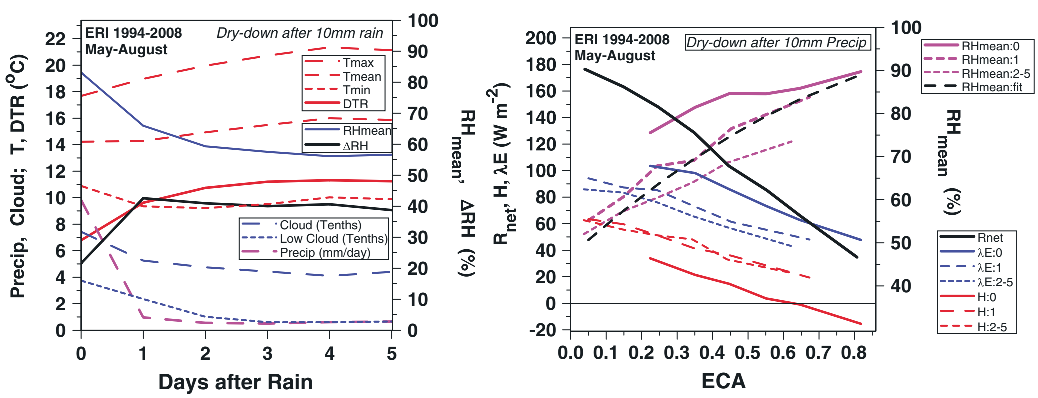

Figure 15. Dry-down after ERA-Interim rain events: (left) change in temperature, DTR, RH_{mean}, ΔRH, cloud, and precipitation and (right) change in surface fluxes and dry-down of RH_{mean}.

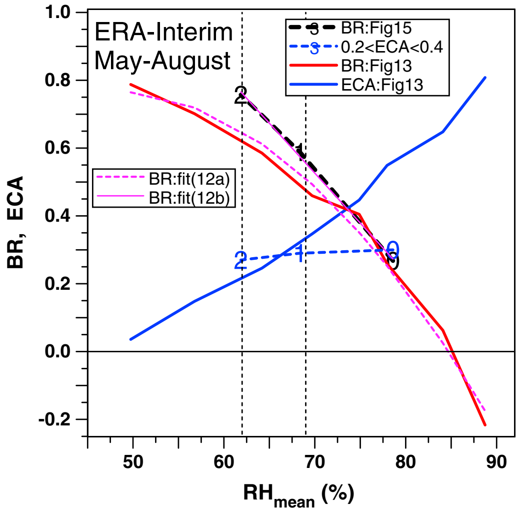

Figure 16. Coupling between RH_{mean} and BR in ERA-Interim.

earlier reanalysis in *Betts et al.* [2007]. The quadratic fit to these Figure 13 BR data is

$$BRa = -0.476 + 0.0524\ RH_{mean} - 0.0005527\ RH_{mean}^2 \quad (12a)$$

[69] A second estimate can be taken from the dry-down sequence in Figure 15, labeled for days 0, 1, and 2. The heavy dashed curve shows the sequential increase of BR as RH_{mean} decreases after rain for fixed cloud cover in the range $0.2 < ECA < 0.4$, and so the $ECA \approx 0.3$ (shown). This plot is quasi-linear, but it includes far fewer days (420) than Figure 13 (1845 days). It is still inhomogeneous because, although cloud cover is constant, day 0 has heavy rain while days 1 and 2 have little rain. The vertical markers at $RH_{mean} = 62$ and 69% are representative of the growing season change in RH_{mean} with land use (Figure 6), and they span the change of RH_{mean} between days 1 and 2. The linear fit is

$$BRb = 2.587 - 0.0294\ RH_{mean} \quad (12b)$$

[70] We will use these two fits relating BR to RH_{mean} in ERA-Interim to partition R_{net} for the Prairie data.

5. Changes in the Surface Energy Budget and Climate With Land Use

[67] The surface climate of the Prairies is a complex system, where the local coupling between land use, boundary layer, clouds, and phenology is coupled to the seasonal cycle as well as to changes in regional and global climate. We have seen, in both the observed seasonal changes in the diurnal climate of the Canadian Prairies with land use and in dry-downs after precipitation, the signature of the local coupling between RH and surface ET. In this section we will use fits from ERA-Interim to couple RH to BR and derive R_{net} from opaque cloud cover, to give a semiquantitative description of the change in the surface energy budget of the Prairies with changing agricultural land use in Saskatchewan.

5.1. Surface Energy Budget: Coupling Between RH and BR

[68] Figure 16 shows two estimates of the coupling between RH_{mean} and BR from ERA-Interim. The solid curves, covering the full range, are replotted from Figure 13 (top row). In this complete set of May–August data, BR increases with RH_{mean}, but at the same time ECA (and precipitation) also increases. Similar relationships were shown for an

5.2. Warm-Season Change With Land Use in Saskatchewan

[71] Figure 17 shows the change in the seasonal cycle with the change in agricultural land use. It is derived from Figure 6 for Saskatchewan by differencing the two time periods, 1953–1991 and 1992–2011, and using fits 7 and 10 for R_{net} and (12) for BR. The vertical markers at DOY = 140 (20 May) and 240 (28 August) are shown as markers for the growing season for annual crops.

[72] Figure 17 (left) shows the change in RH_{mean}, RH:T_{max}, RH:T_{min}, and ΔRH (left-hand scale) and opaque cloud cover (right-hand scale). The light magenta line, which closely follows the change in cloud cover, is the change in RH:fit 3c, corresponding to the change in opaque cloud from the climatology 3c. We see that during the growing season, the actual change in $\delta RH >> \delta RH$:fit 3c, confirming that most of the change in RH comes from higher ET and not from the small increase of cloud cover.

[73] Figure 17 (center) shows the change in T_{max}, T_{mean}, T_{min}, and DTR with the land use change. There is cooling in the growing season and generally warming before DOY = 140 and after DOY = 240. The seasonal change of T_{min} is less than T_{max}, and so the change in DTR has a similar structure to the change of T_{max}. The magenta line is the

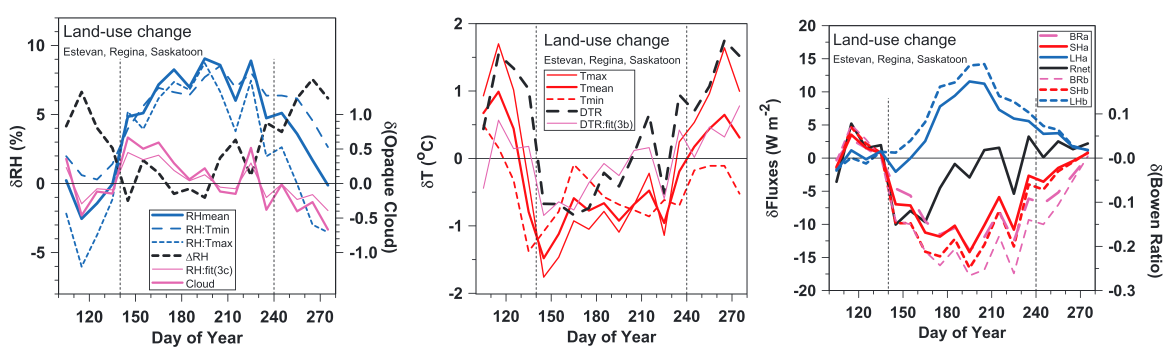

Figure 17. Warm-season changes in temperature, RH, and surface fluxes with land use change.

Table 2. Warm-Season Changes With Land Use Change Between 1953–1991 and 1991–2011[a]

DOY Range	110–139	140–199	200–239	140–239	240–279	110–279
Date Range	4/10 to 5/19	5/20 to 7/18	7/19 to 8/27	5/20 to 8/27	8/28 to 10/6	4/10 to 10/6
T_{max} (°C)	0.79	−1.18	−0.45	−0.89	1.03	−0.14
T_{mean} (°C)	0.21	−0.93	−0.58	−0.79	0.39	−0.33
T_{min} (°C)	−0.52	−0.59	−0.74	−0.65	−0.23	−0.53
DTR (°C)	1.30	−0.59	0.29	−0.24	1.26	0.39
RH:T_{min} (%)	0.8	6.2	7.5	6.7	4.9	5.2
RH_{mean} (%)	−1.3	6.9	7.1	7.0	2.6	4.5
RH:T_{max} (%)	−3.6	6.4	5.0	5.8	−1.0	2.5
ΔRH (%)	4.4	−0.2	2.5	0.9	5.9	2.7
Cloud (Tenths)	−0.24	0.39	−0.03	0.22	−0.34	0.01
P_{LCL}:T_{max} (hPa)	13.3	−26.0	−21.6	−24.2	3.3	−11.1
Precipitation (mm/day)[b]	−0.24	0.50	0.10	0.34	0.02	0.16
R_{net} (W m^{-2})	2.9	−6.0	0.2	−3.5	1.5	−1.2
BRa 12a	0.02	−0.14	−0.15	−0.14	−0.05	−0.09
Ha (W m^{-2})	1.9	−10.3	−7.4	−9.1	−1.2	−5.3
λEa (W m^{-2})	0.7	4.9	7.5	5.9	2.6	4.2
BRb 12b	0.04	−0.20	−0.21	−0.21	−0.08	−0.13
Hb (W m^{-2})	2.5	−12.9	−9.6	−11.6	−1.6	−6.8
λEb (W m^{-2})	0.1	7.5	9.7	8.4	3.0	5.7

[a]A mean of Estevan, Regina, and Saskatoon, except for precipitation.
[b]Also includes Moose Jaw.

change in DTR corresponding to the change in opaque cloud from the climatology 3b. Note that, during the growing season, δDTR is comparable to δDTR:fit 3b, confirming that changes in cloud cover are largely responsible for changes in DTR. However, the growing season changes of T_{max} are larger than DTR, consistent with Figure 11.

[74] Figure 17 (left and center) presents a picture of cooling and moistening with more annual cropping for $140 \le \text{DOY} < 240$ in the growing season in the recent decades, consistent with increased ET. Before DOY = 140 and after DOY = 240, they show warming of T_{max} and a fall of RH:T_{max}, consistent with reduced ET in recent decades. The diurnal ranges DTR and ΔRH both increase.

[75] Figure 17 (right) shows the change in R_{net}, derived from the change in opaque cloud using (7) to (11). We show both fits 12a and 12b for BR and calculate using 4 and 5 the corresponding H and λE (labeled a and b), with the further simplification that $G = 0.1R_{net}$. The change δH closely follows the change δBR. The flux changes using linear fit 12b are a few W m^{-2} larger than using 12a. Despite this uncertainty in the coupling between BR and RH changes, which we have taken from ERA-Interim, an increase of λE and decrease of H is clearly consistent with the increase of RH and the decrease of temperature during the growing season. Our estimates of the reduction of BR between −0.14 and −0.2 during the growing season with increased annual cropping are also consistent with the estimates of *Shrestha et al*. [2012].

[76] The variability across the three stations is visible in Figures 5 and 7. The coherence of the mean changes over the seasonal cycle, shown in Figure 17, is remarkable. Temperature, RH, cloud, and precipitation are all independent measurements, but the picture they present of the impact of the increased annual cropping before, during, and after the growing season is self-consistent.

5.3. Summary of the Surface Climate Changes With Land Use

[77] Table 2 summarizes the mean changes in the diurnal cycle climate, R_{net}, and our two estimates of the changes in the surface energy partition before, during, and after the growing season for the Saskatchewan mean, shown in Figures 6 and 17. We have added the change in precipitation from Figure 7. We show separately the mean changes in the first 60 days of the growing season, when there has been a larger fall in T_{max} and DTR and an increase in cloud cover and precipitation, and the second 40 days, when T_{max} falls less as the cloud change is small. As remarked earlier, RH_{mean} increases about 7% throughout the growing season.

[78] The increased annual cropping with fairly well-defined dates of planting and harvest has sharpened the transitions at the beginning and end of the growing season. This appears most clearly in T_{max} and DTR, which fall in the growing season and increase outside it, and in ΔRH, which changes little in the growing season but increases outside it, as the afternoon minimum in RH (at the time of T_{max}) falls.

[79] Increased opaque cloud during the first 60 days of the growing season reduces R_{net} by 6 W m^{-2} for $140 \le \text{DOY} < 200$, but small cloud reductions outside the growing season mean that for the warm season from $100 \le \text{DOY} < 280$, the change in R_{net} from cloud cover changes is small, of order −1 W m^{-2}. Note that we have not accounted for changes in the surface albedo with land use, as we have assumed a fixed value of $\alpha_s = 0.15$ in 10. The mean increase in precipitation over the 100 day growing season of 0.34 mm/day is a little larger than our estimates of the increased latent heat flux (5.9 to 8.4 W m^{-2}), which convert to an increased evaporation rate of 0.20 to 0.29 mm day^{-1}.

6. Conclusions

[80] The large change in land use in recent decades has substantially changed the summer climate of the Canadian Prairies [*Gameda et al*., 2007]. Although winters have warmed, as the global climate has warmed at higher latitudes, increased ET from the rapid growth of a larger coverage of cropland has cooled and moistened the climate in the growing season. By partitioning the climate station data between the years, 1953–1991 and 1992–2011, we have shown that the changes in the diurnal cycle climate over the warm season are largest in Saskatchewan, where cropland has replaced

summer fallow (where the land was left bare for 1 year) on 15–20% of the land area. During the growing season from 20 May to 27 August, relative humidity has increased by about 7%, while in the first 60 days, 20 May to 18 July, maximum temperatures and the diurnal range of temperature have fallen by 1.2°C and 0.6°C, respectively, and opaque cloud cover has increased by about 4%. We estimated the cloud forcing of the surface radiative fluxes from opaque cloud cover, using fits from *Betts et al*. [2013], and found this increase of cloud cover reduced R_{net} by 6 W m^{-2}.

[81] One important aspect of our analysis has been to use the stratification by opaque cloud cover to separate the impact of changing opaque cloud cover, which changes the surface radiative fluxes, from the impact of changing land use and precipitation on the surface BR. Our composite analysis of precipitation dry-downs shows the recovery of $\mathrm{RH}_{\mathrm{mean}}$ and T_{max} in response to the fall of soil moisture and ET, neither of which are measured. We then used the ERA-Interim grid point data to estimate the coupling between $\mathrm{RH}_{\mathrm{mean}}$ and BR, in order to estimate the changes in sensible and latent heat flux from land use change. We concluded that increased ET from the larger area of annual crops has reduced the surface Bowen ratio between 0.14 and 0.2.

[82] The increase in RH coming from increased ET has been sufficient to lower the LCL and increase θ_E in the afternoon in the growing season and increase daily precipitation by 0.34 mm day^{-1}. This is slightly larger than our estimates for the increase of evaporation, but it suggests that evaporation-precipitation feedback plays a role in the summer climate of the Prairies.

[83] For the month on either side of the growing season, maximum temperatures have increased, increasing the diurnal temperature range and the diurnal range of humidity, while cloud cover has been slightly reduced. These changes are consistent with reduced ET on either side of the growing season for annual crops. For the extended warm-season period from 10 April to 7 October, the increase in opaque cloud during the growing season is offset by the small reductions in cloudiness outside the growing season, so that R_{net} is reduced by only 1 W m^{-2}, assuming a fixed surface albedo.

[84] Outside Saskatchewan, the changes in the seasonal cycle in the Prairies have been similar but smaller, while over the southern boreal forest the seasonal cycle is almost unchanged in temperature and humidity. This lack of any change in summer temperatures in the southern boreal forest is significant but perhaps not surprising, as the Prairies have cooled to the south and the Arctic is warming in summer to the north.

[85] This analysis shows the importance of the seasonal climate transitions in spring and fall that are coupled to the vegetation phenology [*Schwartz*, 1994, 1996; *Betts*, 2011a]. The transitions with snow that are large across the Canadian Prairies [*Betts et al*., 2013] will be analyzed in greater detail in a subsequent paper.

[86] **Acknowledgments.** This research was supported by Agriculture & Agri-Food Canada and by Atmospheric Research. Thanks to John Ball for reprocessing the ERA-Interim data and to Éva Mekis for advice on the precipitation data.

References

AAFC (2011), Agriculture and Agri-Food Canada and Statistics Canada, customized tabulations, Census of Agriculture, CGC Base 1996, 2001, 2006; Census of Agriculture Regular Base 1971, 1976, 1981, 1991. Agriculture and Agri-Food Canada, http://data.gc.ca/data/dataset/573098c4-60d1-4f11-9046-681c219a4d0b.

Betts, A. K. (2004), Understanding hydrometeorology using global models, *Bull. Am. Meteorol. Soc.*, *85*, 1673–1688.

Betts, A. K. (2007), Coupling of water vapor convergence, clouds, precipitation, and land-surface processes, *J. Geophys. Res.*, *112*, D10108, doi:10.1029/2006JD008191.

Betts, A. K. (2009), Land-surface-atmosphere coupling in observations and models. *J. Adv. Model Earth Syst.*, *1*, Art. #4, 18 pp., doi:10.3894/JAMES.2009.1.4, http://james.agu.org/index.php/JAMES/article/view/v1n4/JAMES.2009.1.4.

Betts, A. K. (2011a), Seasonal climate transitions in New England, *Weather*, *66*, 245–248, doi:10.1002/wea.754.

Betts, A. K. (2011b), Vermont climate change indicators, *Weather, Climate and Society*, *3*, 106–115, doi:10.1175/2011WCAS1096.1.

Betts, A. K., and J. H. Ball (1995), The FIFE surface diurnal cycle climate, *J. Geophys. Res.*, *100*, 25,679–25,693.

Betts, A. K., and J. H. Ball (1998), FIFE surface climate and site-average dataset: 1987–1989, *J. Atmos. Sci.*, *55*, 1091–1108.

Betts, A. K., and J. C. Chiu (2010), Idealized model for changes in equilibrium temperature, mixed layer depth and boundary layer cloud over land in a doubled CO_2 climate. *J. Geophys. Res.*, *115*, D19108, doi:10.1029/2009JD012888.

Betts, A. K., and P. Viterbo (2005), Land-surface, boundary layer and cloud-field coupling over the south-western Amazon in ERA-40. *J. Geophys. Res.*, *110*, D14108, doi:10.1029/2004JD005702.

Betts, A. K., J. H. Ball, and J. H. McCaughey (2001), Near-surface climate in the boreal forest, *J. Geophys. Res.*, *106*, 33,529–33,542, doi:10.1029/2001JD900047.

Betts, A. K., B. Helliker, and J. Berry (2004), Coupling between CO_2, water vapor, temperature and radon and their fluxes in an idealized equilibrium boundary layer over land. *J. Geophys. Res.*, *109*, D18103, doi:10.1029/2003JD004420.

Betts, A. K., J. Ball, A. Barr, T. A. Black, J. H. McCaughey, and P. Viterbo (2006), Assessing land-surface-atmosphere coupling in the ERA-40 reanalysis with boreal forest data, *Agric. Forest Meteorol.*, *140*, 355–382, doi:10.1016/j.agrformet.2006.08.009.

Betts, A. K., R. Desjardins, and D. Worth (2007), Impact of agriculture, forest and cloud feedback on the surface energy balance in BOREAS, *Agric. Forest Meteorol.*, *142*, 156–169, doi:10.1016/j.agrformet.2006.08.020.

Betts, A. K., R. Desjardins, and D. Worth (2013), Cloud radiative forcing of the diurnal cycle climate of the Canadian Prairies, *J. Geophys. Res. Atmos.*, *118*, 8935–8953, doi:10.1002/jgrd.50593.

Bootsma, A., and R. De Jong (1988), Estimates of seeding dates of spring wheat on the Canadian Prairies from climate data, *Can. J. Plant Sci.*, *68*(2), 513–517, doi:10.4141/cjps88-062.

Bounoua, L., R. Defries, J. Collatz, P. Sellers, and H. Khan (2002), Effects of land cover conversion on surface climate, *Clim. Change*, *52*, 29–64.

Christidis, N., P. A. Stott, G. C. Hegerl, and R. A. Betts (2013), The role of land use change in the recent warming of daily extreme temperatures, *Geophys. Res. Lett.*, *40*, 589–594, doi:10.1002/grl.50159.

De Ridder, K. (1997), Land surface processes and the potential for convective precipitation, *J. Geophys. Res.*, *102*, 30,085–30,090.

Dee, D. P., 35 co-authors (2011), The ERA-Interim reanalysis: Configuration and performance of the data assimilation system, *Quart. J. Roy. Meteorol. Soc.*, *137*, 553–597, doi:10.1002/qj.828.

Diffenbaugh, N. S. (2009), Influence of modern land cover on the climate of the United States, *Clim. Dyn.*, doi:10.1007/s00382-009-0566-z.

Ecodistrict (2013), Ecodistrict visualization tool.

Fitzjarrald, D. R., O. C. Acevedo, and K. E. Moore (2001), Climatic consequences of leaf presence in the eastern United States, *J. Climate*, *14*, 598–614.

Freedman, J. M., D. R. Fitzjarrald, K. E. Moore, and R. K. Sakai (2001), Boundary layer clouds and vegetation–atmosphere feedbacks, *J. Climate*, *14*, 180–197.

Gameda, S., B. Qian, C. A. Campbell, and R. L. Desjardins (2007), Climatic trends associated with summerfallow in the Canadian Prairies, *Agric. Forest Meteorol.*, *142*, 170–185, doi:10.1016/j.agrformet.2006.03.026.

Georgescu, M., D. B. Lobell, C. B. Field, and A. Mahalov (2013), Simulated hydroclimatic impacts of projected Brazilian sugarcane expansion, *Geophys. Res. Lett.*, *40*, 972–977, doi:10.1029/2012GL054612.

Lu, Y., and L. M. Kueppers (2012), Surface energy partitioning over four dominant vegetation types across the United States in a coupled regional climate model (Weather Research and Forecasting Model 3–Community Land Model 3.5), *J. Geophys. Res.*, *117*, D06111, doi:10.1029/2011JD016991.

Lyons, T. J., R. C. G. Smith, and H. Xinmei (1996), The impact of clearing for agriculture on the surface energy budget, *Int. J. Climatol.*, *16*, 551–558.

Mishra, V., K. A. Cherkauer, D. Niyogi, M. L. Bryan, C. Pijanowski, D. K. Ray, L. C. Bowling, and G. Yang (2010), A regional scale assessment of land use/land cover and climatic changes on water and energy cycle in the upper Midwest United States, *Int. J. Climatol.*, *30*, 2025–2044, doi:10.1002/joc.2095.

Pielke, R. A., Sr. (2001), Influence of the spatial distribution of vegetation and soils on the prediction of cumulus convective rainfall, *Rev. Geophys.*, *39*, 151–177.

Qian, B., X. Zhang, K. Chen, Y. Feng, and T. O'Brien (2009), Observed long-term trends for conditions in Canada, *J. Appl. Meteorol. Climatol.*, *49*, 604–618, doi:10.1175/2009JAMC2275.1.

Qian, B., S. Gameda, X. Zhang, and R. De Jong (2012), Changing growing season observed in Canada, *Clim. Change*, *112*, 339–353, doi:10.1007/s10584-011-0220-8.

Raddatz, R. L. (1998), Anthropogenic vegetation transformation and the potential for deep convection on the Canadian Prairies, *Can. J. Soil Sci.*, *78*, 657–666.

Raddatz, R. L., and J. D. Cummine (2003), Inter-annual variability of moisture flux from the Prairie agro-ecosystem: Impact of crop phenology on the seasonal pattern of tornado days, *Boundary-Layer Meteorol.*, *106*, 283–295.

Schwartz, M. D. (1994), Monitoring global change with phenology: The case of the spring green wave, *Int. J. Biometeor.*, *38*, 18–22.

Schwartz, M. D. (1996), Examining the spring discontinuity in daily temperature range, *J. Climate*, *9*, 803–808.

Schwartz, M. D., and T. R. Karl (1990), Spring phenology: Nature's experiment to detect the effect of "green-up" on surface maximum temperatures, *Mon. Weather Rev.*, *118*, 883–890.

Schwartz, M. D., T. R. Ault, and J. L. Betancourt (2012), Spring onset variations and trends in the continental United States: Past and regional assessment using temperature-based indices. *Int. J. Climatol.*, (wileyonlinelibrary.com), doi:10.1002/joc.3625.

Shrestha, B. M., R. L. Raddatz, R. L. Desjardins, and D. E. Worth (2012), Continuous cropping and moist deep convection on the Canadian Prairies, *Atmosphere*, *3*, 573–590, doi:10.3390/atmos3040573.

Wang, S., Y. Yang, Y. Luo, and A. Rivera (2013), Spatial and seasonal variations in evapotranspiration over Canada's landmass. *Hydrol. Earth Syst. Sci. Discuss.*, *10*, 6107–6151, doi:10.5194/hessd-10-6107-2013 www.hydrol-earth-syst-sci-discuss.net/10/6107/2013/.